Supporting Information

Influence of charge transfer on thermoelectric properties of endohedral metallofullerenes (EMF) complexes

Majed Alshammari,[1] Turki B. Alotaibi,[1] Moteb Altoaibi [1] and Ali K. Ismael[1*]

[1] Department of Physics, Lancaster University, Lancaster, United Kingdom.

Table of contents

Computational details.

1. Optimised DFT Structures of Isolated Moieties

Using the density functional code SIESTA,[1, 2] the optimum geometries of the isolated moieties including Sc_3C_2, Sc_3N and Er_3N were obtained by relaxing the molecules until all forces on the atoms were less than 0.01 eV / Å as shown in Fig. SI.1. A double-zeta plus polarization orbital basis set, norm-conserving pseudopotentials, with an energy cut-off of 250 Rydbergs, defined on the real space grid was used and the local density approximation (GGA) was chosen to be the exchange correlation functional.
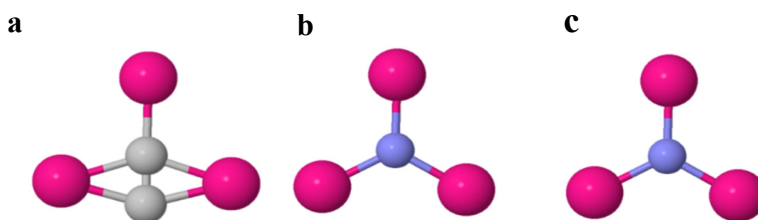
a   b   c

Figure S1. Geometries of an asymmetric Sc_3C_2 (**a**), symmetric Sc_3N and Er_3N moieties (**b** and **c**). Key: C = grey, N = blue and Er = O = red.

Figure SI.1 shows three structures of asymmetric and symmetric metallic moieties. These structures are fully relaxed, and are as follows, **a**: scandium carbide Sc_3C_2 moiety with two different species of atoms including scandium (Sc_3), and carbon (C_2), **b**: scandium carbide Sc_3N moiety with two different species of atoms including scandium (Sc_3), and nitrogen (N), **c**: erbium nitride Er_3C_2 moiety with two different species of atoms including erbium (Er_3). The three metallic moieties were inserted in the C_{80} cag to produce endohedral metallofullerenes (EMF), complexes including $Sc_3C_2@C_{80}$, $Sc_3N@C_{80}$ and $Er_3N@C_{80}$, as shown in Figure S2 (Fig. 2d is an empty fullerene cage). These complexes again fully relaxed under the same conditions to explore their electronic properties later.
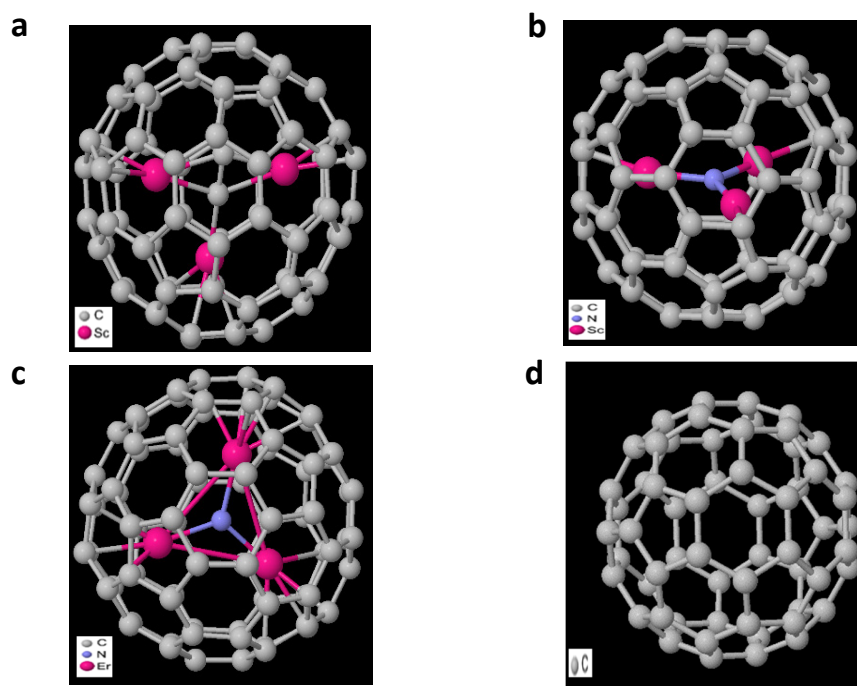
2

Figure S2. Endohedral metallofullerenes and fullerene studied Molecules. Schematic of the three endohedral metallofullerenes (EMFs), namely, **a**: $Sc_3C_2@C_{80}$, **b**: $Sc_3N@C_{80}$, and **c**: $Er_3N@C_{80}$ and an empty fullerene cage **d**: C_{80}.

2. Frontier orbitals of the studied EMFs complexes

To obtain a better understanding of the electronic properties of these complexes (see Figure S2), we will investigate the wave function plots of the $Sc_3C_2@C_{80}$, $Sc_3N@C_{80}$ and $Er_3N@C_{80}$ complexes. The highest occupied molecular orbitals (HOMO), lowest unoccupied orbitals (LUMO), HOMO+1 and LUMO+1 along with their energies are calculated. The blue and red colours correspond to the regions in space of positive and negative orbital amplitude. Figures S3-S5 show the frontier orbitals of the studied complexes, after relaxing the complexes until all forces on the atoms were less than 0.01 eV/Å. The local density approximation (LDA) was chosen to be the exchange correlation functional. We also computed results using GGA and found that the results were comparable with those obtained using LDA.[3-5]

Figures S3-S5 illustrate the theoretical frontier orbitals of the isolated complexes. DFT tends to underestimate the HOMO-LUMO gap,[6, 7] which is why the calculated gaps in Table S1 are smaller than the optically-measured gaps reported in.[8]

2.1. Frontier orbitals of $Sc_3C_2@C_{80}$ complex

E_F=-4.05 eV

HOMO =-4.36 eV   LUMO =-3.89 eV

HOMO-1=-3.95 eV   LUMO+1=-2.97 eV

Figure S3. Wave function plots of $Sc_3C_2@C_{80}$ complex. **Top panel**: fully optimised geometry of $Sc_3C_2@C_{80}$ EMF. **Lower panel**: HOMO, LUMO, HOMO-1, LUMO+1 of $Sc_3C_2@C_{80}$ complex along with their energies.

2.2. Frontier orbitals of $Sc_3N@C_{80}$ complex

E_F=-3.58 eV

HOMO=-4.35 eV

LUMO=-2.83 eV

HOMO-1=-4.39 eV

LUMO+1=-2.55 eV

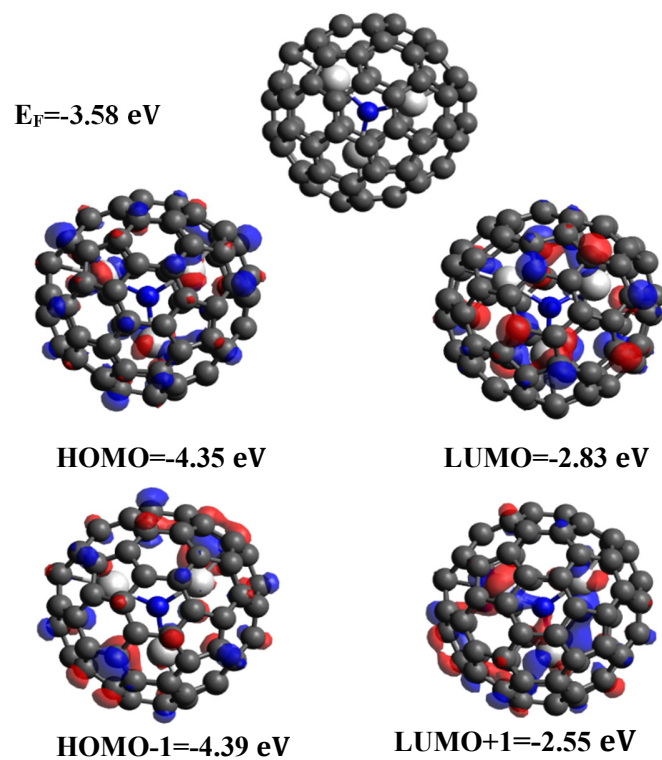**Figure S4.** Wave function plots of $Sc_3N@C_{80}$ complex. **Top panel**: fully optimised geometry of $Sc_3C_2@C_{80}$ EMF. **Lower panel**: HOMO, LUMO, HOMO-1, LUMO+1 of $Sc_3N@C_{80}$ complex along with their energies.

2.3. Frontier orbitals of Er₃N@C₈₀ complex

E_F=-3.91 eV

HOMO =-3.94 eV   LUMO =-3.84 eV

HOMO-1=-3.95 eV   LUMO+1=-3.74 eV

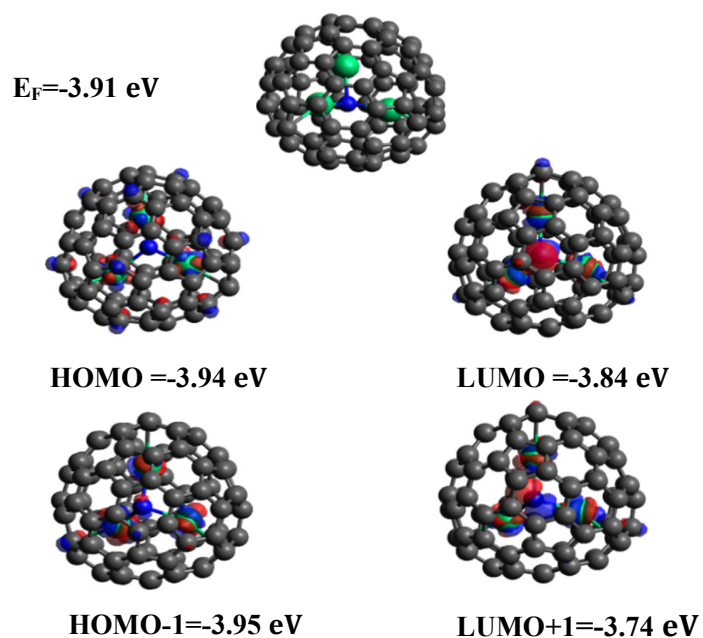**Figure S5.** Wave function plots of Er$_3$N@C$_{80}$ complex. **Top panel**: fully optimised geometry of Sc$_3$C$_2$@C$_{80}$ EMF. **Lower panel**: HOMO, LUMO, HOMO-1, LUMO+1 of Er$_3$N@C$_{80}$ complex along with their energies.

3. Charge transfer analyses

Net atomic charge is a common idea in all chemical sciences. It is difficult to imagine learning chemistry without discussing net atomic charges.[9] For example, experiments measuring the water molecule's dipole moment imply a negative net atomic charge on its oxygen atom and a positive net atomic charge on each of its two hydrogen atoms.[10] Net atomic charge also plays an important role in solid state physics, where oxygen atoms in solid oxides carry negative net atomic charges to enable oxygen ion transport.[11] There are many methods to calculate the charge transfer in Density Functional Theory. In this chapter, I am going to focus on three methods, that are implemented in SIESTA code, including Mulliken populations, Hershfield and Voronoi charge analyses.

Here, we will investigate the electrical properties of the 3 EMFs complexes first in the gas phase, then we repeat the same calculations, but on an Au substrate. Electrons are expected to be transferred from the donor moiety (the metallic moetiy) to the acceptor (the cage). The three methods Mulliken, Hirshfeld and Voronoi) will be used to determine the charge transfer from the donor to the acceptor.

3.1. Charge transfer analyses of EMFs complexes in gas phase

Tables S1, show, the charge transfer from the metallic moieties to the Ih-C_{80} cage. The second row of Table S1, illustrates that the metallic moiety Sc_3C_2 loses (+) in total 1.4 electrons. 1.14 is the net charge that has been gained (-) by the Ih-C_{80} cage, the difference of 0.26 electrons remains within the metallic moiety Sc_3C_2, (specifically by the C_2 atoms), these figures estimated by the Mulliken method. Hirshfeld and Voronoi charge analyse follow a similar trend; the net charges are 1.15 and 1.06 electrons and the differences are gained by the C_2 atoms 0.32, 0.34 electrons respectively.

The third row of Table S1, illustrates that the metallic moiety Sc_3N loses (+) in total 1.5 electrons. 1.26 is the net charge that has been gained (-) by the Ih-C_{80} cage, the difference of 0.24 electrons remains within the metallic moiety Sc_3N (specifically by the N atom), these figures estimated by the Mulliken method. Hirshfeld and Voronoi charge analyse follow a similar trend; the net charges are 1.31 and 1.27 electrons and the differences are gained by the C_2 atoms 0.33, 0.31 electrons respectively.

The last row of Table S1, illustrates that the metallic moiety Er_3N loses (+) in total 6.96 electrons. 5.14 is the net charge that has been gained (-) by the Ih-C_{80} cage, the difference of 1.82 electrons remains within the metallic moiety Er_3N (specifically by the N atom), these figures estimated by the Mulliken method. Hirshfeld and Voronoi charge analyse follow a similar trend; the net charges are 7.48 and 7.14 electrons and the differences are gained by the C_2 atoms 1.34, 1.32 electrons respectively.

It is worth mentioning that, the charge transferred from the metallic moetiy to the cage and the charge effected on the electrical conductance G and Seebeck coefficients S.

Table S1: Charge transfer analyses using Mulliken, Hirshfeld and Voronoi methods of $Sc_3C_2@C_{80}$, $Sc_3N@C_{80}$ and $Er_3N@C_{80}$ complexes. The total number of electrons transferred from metallic moieties (with a charge of $+|e|$), to $Ih-C_{80}$ cages (with a charge of $-|e|$), to form complexes. Note: loss-gain differences gain by C_2, N and N (numbers in brackets), of $Sc_3C_2@C_{80}$, $Sc_3N@C_{80}$ and $Er_3N@C_{80}$ complexes in gas phase.

Metallic Moiety	Mulliken charge		Hirshfeld charge		Voronoi charge	
	Moiety	C_{80} cage	Moiety	C_{80} cage	Moiety	C_{80} cage
Sc_3C_2	+1.40	-1.14	+1.15	-0.83	+1.06	-0.72
Sc_3N	+1.50	-1.26	+1.31	-0.98	+1.27	-0.96
Er_3N	+6.96	-5.14	+7.48	-6.14	+7.14	-5.82

3.2. Charge transfer analyses of EMFs complexes on a gold (111), surface

The analyses here are built on the 3 factors, namely a metallic moiety, a cage and a gold substrate. Table S2, shows the amount of charge transfer from the metallic moieties Sc_3C_2 and Au substrate to $Ih-C_{80}$ cage. The second of Table S2, illustrates that the metallic moiety Sc_3C_2 and Au lose (+) in total 1.63 electrons. 1.39 is the net charge that has been gained (-) by the $Ih-C_{80}$ cage, the difference of 0.24 electrons resides within the metallic moiety Sc_3C_2 (specifically by the C_2 atoms), these figures estimated by the Mulliken method. Hirshfeld and Voronoi charge analyse follow a similar trend; the net charges are 1.13 and 1.15 electrons and the differences are gained by the C_2 atoms 0.32, 0.36 electrons respectively.

The third of Table S2, illustrates that the metallic moiety Sc_3N and Au lose (+) in total 2.37 electrons. 2.09 is the net charge that has been gained (-) by the $Ih-C_{80}$ cage, the difference of 0.24 electrons resides within the metallic moiety Sc_3N (specifically by the N atom), these figures estimated by the Mulliken method. Hirshfeld and Voronoi charge analyse follow a similar trend; the net charges are 1.30 and 1.28 electrons and the differences are gained by the C_2 atoms 0.32, 0.26 electrons respectively.

The last of Table S2, illustrates that the metallic moiety Er_3N and Au lose (+) in total 6.77 electrons. 5.20 is the net charge that has been gained (-) by the $Ih-C_{80}$ cage, the difference of 0.28 electrons resides within the metallic moiety Er_3N (specifically by the N atom), these figures estimated by the Mulliken method. Hirshfeld and Voronoi charge analyse follow a similar trend; the net charges are 7.24 and 6.95 electrons and the differences are gained by the N atoms 1.44, 1.35 electrons respectively.

Table S2: Charge transfer analyses using Mulliken, Hirshfeld and Voronoi methods of $Sc_3C_2@C_{80}$, $Sc_3N@C_{80}$ and $Er_3N@C_{80}$ complexes. The total number of electrons transferred from metallic moieties (with a charge of +|e|), to $Ih-C_{80}$ cages (with a charge of -|e|), to form complexes. Note: loss-gain differences gain by C_2, N and N (numbers in brackets), of $Sc_3C_2@C_{80}$, $Sc_3N@C_{80}$ and $Er_3N@C_{80}$ complexes on an Au (111), surface.

Metallic Moiety	Mulliken charge		Hirshfeld charge		Voronoi charge	
	Moiety + Au	$Ih-C_{80}$ cage	Moiety + Au	$Ih-C_{80}$ cage	Moiety + Au	$Ih-C_{80}$ cage
Sc_3C_2	+1.63	-1.39	+1.13	-0.81	+1.15	-0.79
Sc_3N	+2.37	-2.09	+1.30	-0.98	+1.28	-1.02
Er_3N	+6.77	-5.20	+7.24	-5.80	+6.95	-5.60

4. Binding energies of EMFs on a gold surface

To calculate the optimum binding distance for EMFs complexes on the gold (111) surface, we use DFT, combined with the counterpoise method, which removes basis set superposition errors (BSSE). As shown by the example of $Sc_3C_2@C_{80}$ in Figure S6, the distance z is defined as the distance between the Au surface and the nearest C atom of the C_{80} cage (see the white double-arrow on the right panel of Figure S6).

The ground state energy of the total system is calculated using SIESTA[1] and is denoted E_{AB}^{AB}. Here the gold leads consist of 3 layers of 25 atoms. The $Sc_3C_2@C_{80}$ molecule is defined as monomer A and the gold electrodes as monomer B. The binding energy of each molecule is then calculated in a fixed basis, which is achieved through the use of ghost atoms in SIESTA. Hence the energy of the isolated $Sc_3C_2@C_{80}$ in the presence of the fixed basis is defined as E_A^{AB} and for the isolated gold is E_B^{AB}. The energy difference ($\Delta(z)$)

between the isolated entities and their total energy when placed a distance z apart is then calculated using the following equation:

$$\text{Energy difference} = \Delta(z) = E_{AB}^{AB}(z) - E_A^{AB} - E_B^{AB} \tag{S1}$$

As shown by the Figure S6, the equilibrium distance for $Sc_3C_2@C_{80}$, corresponding to the minimum energy difference, is found to be approximately 2.5 Å, which is comparable with a value of 2.4 Å reported in Ref. [12].
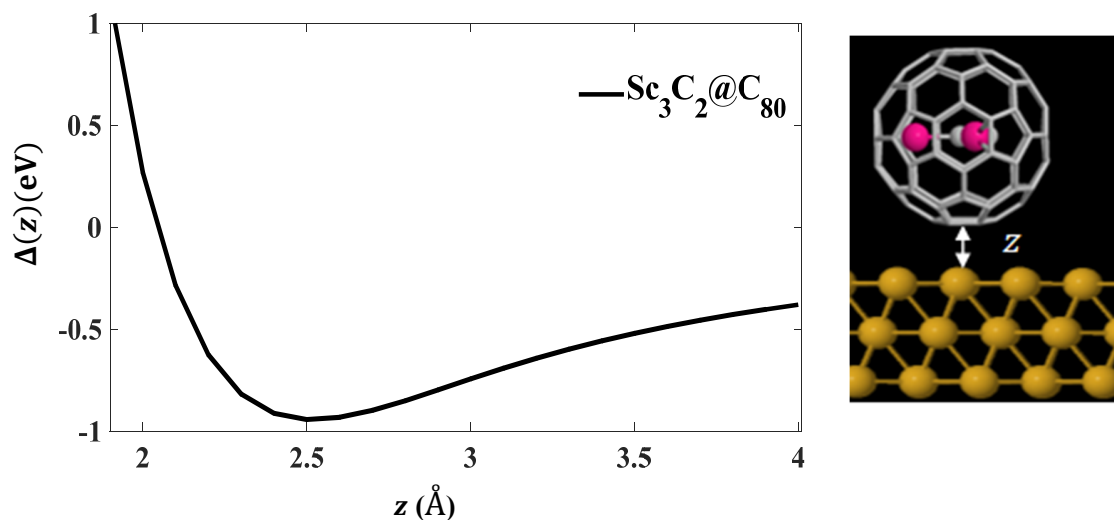

Figure S6. $Sc_3C_2@C_{80}$ on a gold surface (Right panel). Energy difference of $Sc_3C_2@C_{80}$/gold complex as a function of molecule-gold distance. The equilibrium distance corresponding to the energy minimum is found to be approximately 2.5 Å (Left panel).

5. Calculated thermopower as a function of orientation in the horizontal rotation axis (θ)

To calculate the thermopower of these molecular junctions, it is useful to introduce the non-normalised probability distribution $P(E)$ defined by

$$P(E) = -T(E)\frac{df(E)}{dE} \tag{S2}$$

where $f(E)$ is the Fermi-Dirac function and $T(E)$ is the transmission coefficients and whose moments L_i are denoted as follows

$$L_i = \int dE P(E)(E - E_F)^i \tag{S3}$$

where E_F is the Fermi energy. The Seebeck coefficient, S, is then given by

$$S(T) = -\frac{1}{eT}\frac{L_1}{L_0} \tag{S4}$$

where e is the electronic charge.

Note that in ref [75] of the main manuscript, equation (50), contains a typographical error and is not the formula evaluated by the Gollum code. The formula evaluated by Gollum is

$$S^e(T) = \frac{-1}{eT}\frac{L_1}{L_0}$$

where

$$L_i = \int dE P(E)(E - E_F)^i$$

and

$$P(E) = -T(E)\frac{df(E)}{dE}$$

In this expression, $T(E) = \frac{T_{up}(E) + T_{down}(E)}{2}$, where $T_{up}(E)$ and $T_{down}(E)$ are transmission coefficients for the separate spin channels and it is assumed that there is no spin-flip scattering.

This equation describes the linear response regime and is consistent with Onsager reciprocal relations.

Figures S14 and S15 show the average Seebeck coefficient S evaluated at room temperature for different orientation angles of θ for $Sc_3C_2@C_{80}$ and $Sc_3N@C_{80}$.

Figure S7. Seebeck coefficient S as a function of Fermi energy at 60 different orientations angles θ of $Sc_3C_2@C_{80}$, for a tip-substrate distance of 2.5 Å.

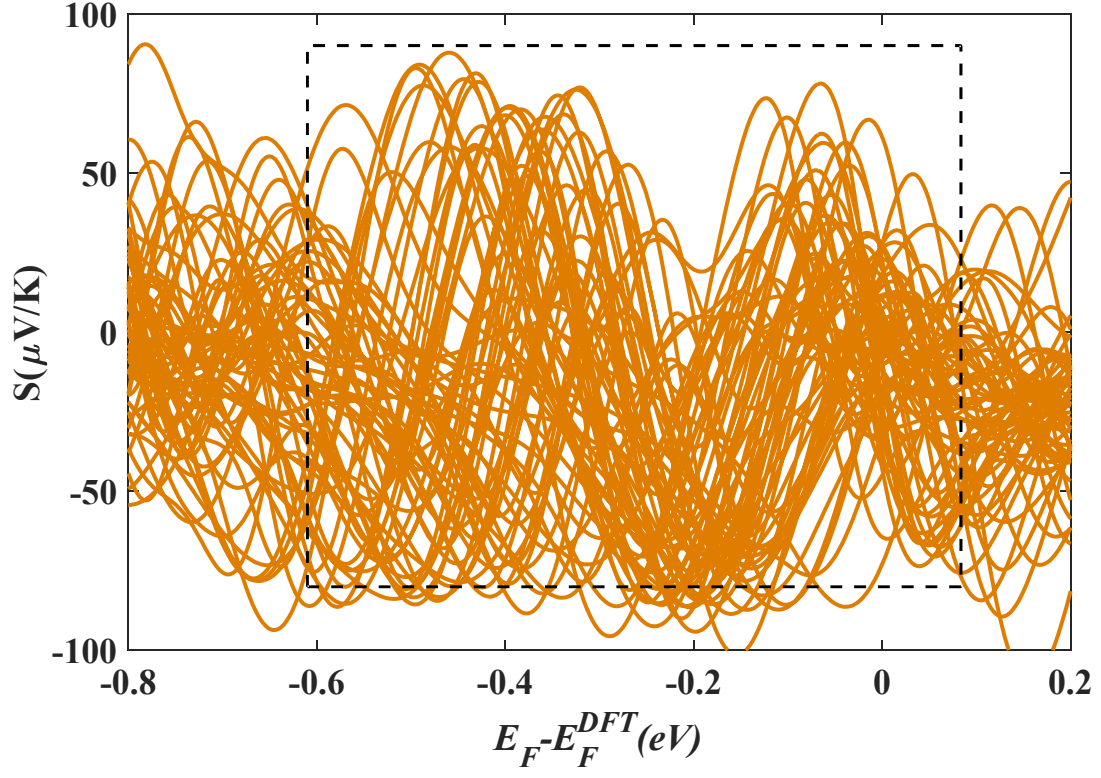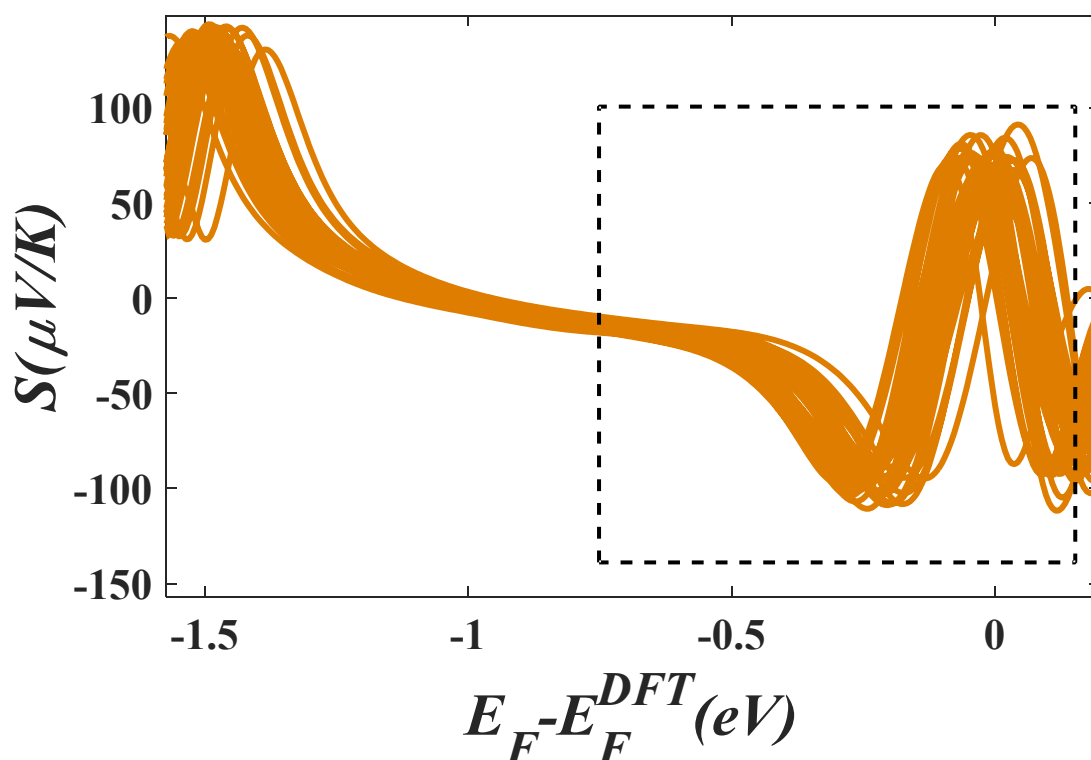**Figure S8.** Seebeck coefficients *S* as a function of Fermi energy at 60 different orientation angles θ of Sc$_3$N@C$_{80}$ for a tip-substrate distance of 2.5 Å

References

1.   Soler, J. M.; Artacho, E.; Gale, J. D.; García, A.; Junquera, J.; Ordejón, P.; Sánchez-Portal, D. J. J. o. P. C. M., The SIESTA method for ab initio order-N materials simulation. *Journal of Physics: Condensed Matter* **2002,** *14* (11), 2745.

2.   Emilio, A.; Anglada, E.; Diéguez, O.; Gale, J. D.; García, A.; Junquera, J.; Martin, R. M.; Ordejón, P.; Pruneda, J. M.; Sánchez-Portal, D.; Soler, J. M., The SIESTA method; developments and applicability. *J. Phys.: Condens. Matter* **2008,** *20* (6), 064208.

3.   Herrer, I. L.; Ismael, A. K.; Milan, D. C.; Vezzoli, A.; Martín, S.; González-Orive, A.; Grace, I.; Lambert, C.; Serrano, J. L.; Nichols, R. J., Unconventional single-molecule conductance behavior for a new heterocyclic anchoring group: pyrazolyl. *The journal of physical chemistry letters* **2018,** *9* (18), 5364-5372.

4.   Ismael, A. K.; Wang, K.; Vezzoli, A.; Al-Khaykanee, M. K.; Gallagher, H. E.; Grace, I. M.; Lambert, C. J.; Xu, B.; Nichols, R. J.; Higgins, S. J., Side-Group-Mediated Mechanical Conductance Switching in Molecular Junctions. *Angewandte Chemie International Edition* **2017,** *56* (48), 15378-15382.

5.   Markin, A.; Ismael, A. K.; Davidson, R. J.; Milan, D. C.; Nichols, R. J.; Higgins, S. J.; Lambert, C. J.; Hsu, Y.-T.; Yufit, D. S.; Beeby, A., Conductance Behavior of Tetraphenyl-Aza-BODIPYs. *The Journal of Physical Chemistry C* **2020,** *124* (12), 6479-6485.

6.   Lof, R.; Van Veenendaal, M.; Koopmans, B.; Jonkman, H.; Sawatzky, G., Band gap, excitons, and Coulomb interaction in solid C 60. *Physical review letters* **1992,** *68* (26), 3924.

7.   Hung, Y.-C.; Jiang, J.-C.; Chao, C.-Y.; Su, W.-F.; Lin, S.-T., Theoretical Study on the Correlation between Band Gap, Bandwidth, and Oscillator Strength in Fluorene-Based Donor– Acceptor Conjugated Copolymers. *The Journal of Physical Chemistry B* **2009,** *113* (24), 8268-8277.

8.   Ismael, A. K.; Rincón-García, L.; Evangeli, C.; Dallas, P.; Alotaibi, T.; Al-Jobory, A. A.; Rubio-Bollinger, G.; Porfyrakis, K.; Agraït, N.; Lambert, C. J., Exploring seebeck-coefficient fluctuations in endohedral-fullerene, single-molecule junctions. *Nanoscale Horizons* **2022,** *7*, 616-625.

9.   Shusterman, A. J.; Hoistad, L. M., Teaching Chemistry with Electron Density Models. 2. Can Atomic Charges Adequately Explain Electrostatic Potential Maps? *The Chemical Educator* **2001,** *6* (1), 36-40.

10.   Clough, S. A.; Beers, Y.; Klein, G. P.; Rothman, L. S., Dipole moment of water from Stark measurements of H2O, HDO, and D2O. *The Journal of Chemical Physics* **1973,** *59* (5), 2254-2259.

11.   Skinner, S. J.; Kilner, J. A., Oxygen ion conductors. *Materials Today* **2003,** *6* (3), 30-37.

12.   Rincón-García, L.; Ismael, A. K.; Evangeli, C.; Grace, I.; Rubio-Bollinger, G.; Porfyrakis, K.; Agraït, N.; Lambert, C. J., Molecular design and control of fullerene-based bi-thermoelectric materials. *Nature materials* **2016,** *15* (3), 289-293.